This article has been accepted for publication in a future issue of this journal, but has not been fully edited. Content may change prior to final publication. Citation information: DOI 10.1109/TIE.2017.2772152, IEEE Transactions on Industrial Electronics

Cost-Effective Current Measurement Technique for Four-Phase SRM Control by Split Dual Bus Line Without Pulse Injection and Voltage Penalty

Chun Gan, *Member, IEEE*, Qingguo Sun, Nan Jin, *Member, IEEE*, Leon M. Tolbert, *Fellow, IEEE*, Zhibin Ling, *Member, IEEE*, Yihua Hu, *Senior Member*, and Jianhua Wu

***Abstract*—This paper proposes a simple and cost-effective current measurement technique for four-phase switched reluctance motor (SRM) control, by splitting the dual bus line of the converter, without pulse injection and voltage penalty. Only two hall-effect sensors are utilized, where one is installed in the upper bus to measure two phase currents, and another one is placed in the lower bus to measure another two phase currents. In order to realize independent current measurement in the whole turn-on region, switching functions are redesigned so that upper switches of two phases act as the choppers, while lower switches of the other two phases are employed as the choppers. Compared to traditional drives, the developed system requires only two hall-effect sensors in the dual bus line, without a need for individual phase sensors or additional devices, which reduces the cost and volume for SRM drives. Furthermore, compared to the single-sensor based current measurement scheme, the proposed method has no need to implement pulse injection and will not cause any voltage penalty and current distortion, which also improve the current measurement accuracy and system performance. Simulation and experiments carried out on a 150-W four-phase 8/6 SRM confirm the effectiveness of the proposed technique.**

***Index Terms*—Current measurement, split dual bus line, cost-effective, reduced sensors, SRM control.**

Manuscript received April 3, 2017; revised October 2, 2017; accepted October 13, 2017. *(Corresponding author: Nan Jin.)*

C. Gan is with the Department of Electrical Engineering and Computer Science, University of Tennessee, Knoxville, TN 37996, USA, and also with the College of Electrical Engineering, Zhejiang University, Hangzhou 310027, China (e-mail: cgan@utk.edu).

Q. Sun and J. Wu are with the College of Electrical Engineering, Zhejiang University, Hangzhou 310027, China (e-mail: lwsunqg@163.com; hzjhwu@163.com).

N. Jin is with the College of Electric and Information Engineering, Zhengzhou University of Light Industry, Zhengzhou 450002, China, and also with the Department of Electrical Engineering and Computer Science, University of Tennessee, Knoxville, TN 37996, USA (e-mail: njin3@utk.edu).

L. M. Tolbert is with the Department of Electrical Engineering and Computer Science, University of Tennessee, Knoxville, TN 37996, USA (e-mail: tolbert@utk.edu).

Zhibin Ling is with the Department of Electrical Engineering, Shanghai Jiao Tong University, Shanghai 200240, China (e-mail: lingzhibin@sjtu. edu.cn).

Y. Hu is with the Department of Electronic and Electrical Engineering, University of Liverpool, Liverpool L69 3BX, U.K. (e-mail: y.hu35@liverpool.ac.uk).

I. Introduction

In recent years, electric vehicles (EVs) and hybrid EVs (HEVs) have received much attention, owing to the high demand of fuel efficiency and exhaust gas emissions [1]-[5]. Permanent-magnet synchronous machines (PMSMs) have proven to be a popular solution, due to high efficiency and high torque density [6]-[8]. However, the permanent magnets fabricated from rare-earth materials bring about poor stability in high temperatures and high cost [9], [10]. Also, the mining of rare earth materials leads to serious environmental issues. To overcome the shortcomings of PMSMs, many efforts have been devoted to developing motors with reduced rare-earth content or rare-earth-free motors for future traction drives [11], [12].

As a typical representative of the rare-earth-free motors, switched reluctance motors (SRMs) have received significant interests in recent years, due to their characteristics of low cost, high torque, high reliability, wide-speed range, and good fault tolerance ability. Hence, they are a competitive candidate for high-speed, high-temperature, and safety-critical applications, such as home appliances [13], [14] and EVs/HEVs [15]-[25]. In SRMs, only silicon steel and stator windings are needed, without any rotor windings and permanent magnets, thus the motor configuration is much simpler and more robust compared to PMSMs, which gives these motors the ability to work in a harsh environment. Hence, they are a competitive candidate for high-speed, high-temperature, and safety-critical applications.

In a current-controlled motor drive, the phase currents are needed not only for feedback control but also for overcurrent protection. Therefore, the phase current information is very important in a highly reliable motor system. Conventionally, individual hall-effect current sensors are installed in each phase to measure the current information, which not only increases the cost and volume of the system but also decreases the system reliability, especially for multiphase inverters/converters. Considering this point, advanced current measurement technologies have been developed to reduce the current sensors for different motor drives or inverter topologies [26]-[35].

Three-phase current reconstruction scheme for induction motor (IM) drives is proposed in [26], by detecting the dc-link current based on the stator winding equations and motor states. In [27], a new phase current reconstruction scheme using dc current information with reduced immeasurable area and common mode voltage is proposed for IM drives, by employing tristate pulse-width modulation (PWM) technique. In [28], a switching-state phase-shift method is presented to reconstruct

0278-0046 (c) 2017 IEEE. Personal use is permitted, but republication/redistribution requires IEEE permission. See http://www.ieee.org/publications_standards/publications/rights/index.html for more information.

This article has been accepted for publication in a future issue of this journal, but has not been fully edited. Content may change prior to final publication. Citation information: DOI 10.1109/TIE.2017.2772152, IEEE Transactions on Industrial Electronics

three-phase currents for PMSM drives using a single current sensor in the dc link, which reduces the cost and improves the reliability of motor systems. A hybrid method consisting of space vector modulation method and the PWM method without using null switching states is put forward in [29] to reduce the current distortion and extend the current reconstruction range for three-phase inverters. In [30], zero voltage vector sampling method is reported for phase current reconstruction of PMSM drives, by placing the single current sensor at a novel position to detect the current in two zero voltage vectors, without modifying PWM signals. A new space vector PWM scheme is presented in [31] to reconstruct phase currents using neutral point current measurement in three-level T-type converters. A minimum voltage injection method is proposed in [32], to expand the current measurable areas and minimize the distortion in output voltages for phase current reconstruction of three-level inverters.

For SRMs, some advanced current detection and phase current reconstruction schemes have been proposed to reduce the number of required hall-effect sensors [33]-[35]. Phase current detection using a single current sensor is first introduced in [33] by using complex logic circuits to insert detection states, which decreases the sampling accuracy and reliability. To improve this scheme, a double high-frequency pulse injection method is proposed in [34] to reconstruct each phase current from the dc-link current when the phase currents are overlapped. In [35], an online sensorless position estimation technique is proposed using only one current sensor. The instantaneous rotor position is estimated from the excitation current that is decoupled from the bus current by employing pulse injection. However, in terms of single-sensor based schemes, phase current measurement is achieved by pulse injection and phase-shifting of PWM signals. The implementation of pulse injection will inevitably cause the voltage penalty and additional switching loss, due to the added switching actions. The voltage penalty leads to current distortion and decreases the measurement accuracy. Also, the current sensor should be reselected with larger measuring range, due to the overlapped currents flowing through the sensor. A more promising current measurement scheme should satisfy the following requirements:

1) accurate phase current measurement for control;
2) little change to traditional converter topologies;
3) no voltage penalty and no current distortion;
4) no decrease in system efficiency and no increase in output torque ripple;
5) relatively low cost without added hardware circuit.

This paper proposes a simple and cost-effective current measurement technique for four-phase SRM control, by splitting the dual bus lines with reduced hall-effect sensors, to match the above requirements. In the proposed scheme, the upper and lower bus lines are both split into two parts, and two current sensors are utilized in the split dual bus line, respectively, to detect the upper and lower bus currents. In order to measure the phase current in the whole turn-on region, switching functions for all the switches are redesigned that the lower switches of two phases are used as the choppers, while the upper switches of the other two phases act as the choppers. Then, all the phase currents can be further obtained from the two sampled bus currents for current regulation, by using the corresponding conduction information of each phase.

Compared to traditional SRM drives, the developed system requires only two hall-effect sensors in the dual bus line, without a need for individual sensors or additional detection devices, which considerably reduces the cost and volume of the system. Furthermore, compared to the single-sensor based scheme [33], [34], this scheme is relatively easy and there is no need to implement pulse injection, which will not cause any voltage penalty, current distortion, and reduction in current measurement accuracy and system efficiency. There is a tradeoff between the two-sensor scheme without pulse injection and single-sensor scheme with pulse injection. In terms of the reliability, although one more sensor is used, there is no need to inject additional pulses into drive signals, which will increase the system reliability. In terms of the complexity, the currents do not need to be sampled at specific sampling instants under pulse injection. Therefore, the current sampling is really simple in the proposed scheme. Also, there is no need to reselect the hall-effect sensors with larger measuring ranges, due to non-overlapped currents flowing through the sensors. Hence, the complexity can be reduced compared to the single-sensor scheme. The simulation and experimental results on a 150-W four-phase 8/6 SRM are presented to confirm the effectiveness of the proposed technique.

II. Proposed Current Measurement Technique

A. Operational Modes of SRM Drives

Conventionally, asymmetrical half-bridge converters are usually employed in SRM drives due to their phase independent characteristics, which lead to high reliability and good fault tolerant ability. Fig. 1 presents a four-phase 8/6-pole SRM drive, including a converter for energy conversion, current measurement for system control and protection, position detection for speed calculation and phase commutation, and a motor. The phase current measurement is an important part, which not only determines the control performance but also affects the fault diagnosis accuracy.

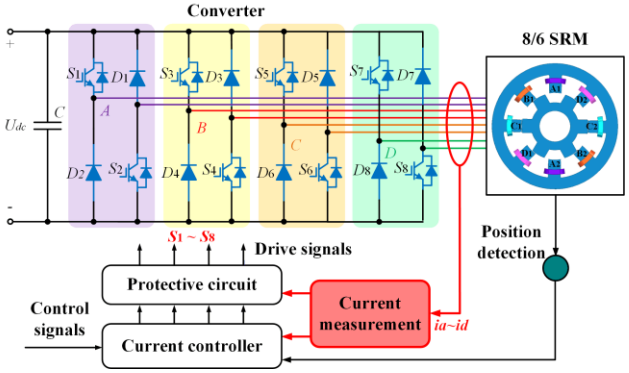

Fig. 1. Four-phase 8/6-pole SRM drive.

The basic operational modes of the asymmetrical half-bridge converter are shown in Fig. 2, including conduction mode, freewheeling mode, and demagnetization mode, where the upper switch is employed as the chopper. When switches S_3 and S_4 are both turned on, phase B is energized by the power source, where it works in the conduction mode, as shown in Fig. 3(a);

0278-0046 (c) 2017 IEEE. Personal use is permitted, but republication/redistribution requires IEEE permission. See http://www.ieee.org/publications_standards/publications/rights/index.html for more information.

This article has been accepted for publication in a future issue of this journal, but has not been fully edited. Content may change prior to final publication. Citation information: DOI 10.1109/TIE.2017.2772152, IEEE Transactions on Industrial Electronics

when S_3 is turned off and S_4 is on, the phase B current will flow through S_4 and diode D_4 to form a zero voltage loop, and it works in the freewheeling mode, as shown in Fig. 3(b); when S_3 and S_4 are both turned off, the phase B current will flow through D_3 and D_4 to feedback to the dc-link, where phase B works in the demagnetization mode, as shown in Fig. 3(c). In the phase turn-on region, the conduction mode and freewheeling mode are both included, and the current in this region is defined as the excitation current in this paper.

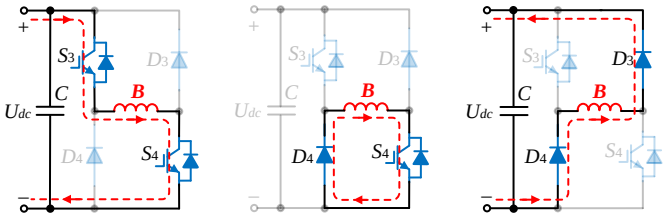

Fig. 2. Operational modes of the asymmetrical half-bridge converter in one current cycle. (a) Conduction. (b) Freewheeling. (c) Demagnetization.

In current regulation control, the soft chopping scheme, where the upper switch acts as a chopper and the lower switch remains closed in the phase turn-on region, is usually employed to reduce the switching loss. When a phase conducts, the upper and lower switches are both turned on to increase the current rapidly. When the current reaches the maximum of the current hysteresis width, the upper switch is turned off and the lower switch remains on to let the phase work under freewheeling mode, and then the current decreases. If the current reaches the minimum of the current hysteresis width, the upper and lower switches are both turned on again to increase the current. When the phase should be turned off to implement phase commutation, the upper and lower switches are both turned off simultaneously, and the current decreases quickly to zero due to the negative voltage on the phase winding.

B. Analysis of Phase Currents

The phase currents and switching signals for a four-phase SRM under current regulation control are illustrated in Fig. 3, where i_a, i_b, i_c and i_d are the phase currents for phases A, B, C, and D, respectively, and S_1~S_8 are the switching signals for the four phases. θ_1 and θ_3 are the turn-on angles of phases B and C, respectively, θ_2 and θ_4 are the turn-off angles of phases A and B, respectively, and θ_5 is the current ending angle of phase B.

Taking phase B for example, Regions I~IV represent a whole current period for phase B. In Region I, phases A and B both conduct, and their excitation currents are overlapped. In Region II, phase A is turned off, and the demagnetization current of phase A and excitation current of phase B overlaps. In Region III, phase C is turned on and phase B still conducts, the excitation currents of these two phases are in overlap condition. In Region IV, the sum current contains the demagnetization current of phase B and excitation current of phase C, due to phase B turning off.

The phase shift angle between the turn-on angles of the adjacent phases is equal to the stroke angle, given by

$$\theta_{ps} = \frac{360^{\circ}}{m \times N_r} \tag{1}$$

where m is the number of motor phases, N_r is the number of rotor poles. Hence, the phase shift angle is determined by the number of motor phases and number of rotor poles. For a four-phase 8/6 SRM, m=4 and N_r=6. Therefore, θ_{ps}=15°.

θ_3 and θ_1 satisfy

$$\theta_3 = \theta_1 + \theta_{ps} = \theta_1 + 15^{\circ} \tag{2}$$

Because each phase shares the same current controller, the turn-on region for each phase is the same and the phase current has the same shape with 15° phase shift between each other. Hence, the overlapped regions between two adjacent phases are the same.

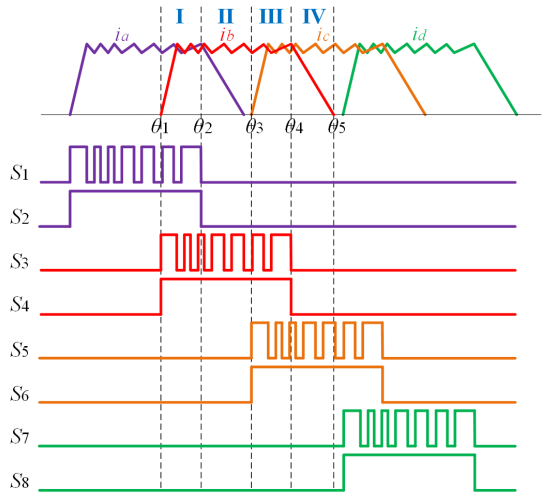

Fig. 3. Phase currents and switching signals for a four-phase SRM.

The sum of the phase currents in the rotor position region of θ_1~θ_5 can be expressed as

$$i_{bus} = \begin{cases} i_a + i_b, & \theta_1 < \theta \le \theta_3 \\ i_b + i_c, & \theta_3 < \theta \le \theta_5 \end{cases} \tag{3}$$

The demagnetization currents are not used for current regulation control, which do not need to be measured. Hence, if all the demagnetization currents can be removed from the sum of the phase currents, the current sampling will be simpler. The sum of the phase currents excluding all the demagnetization currents can be expressed as (4) in the rotor position region θ_1~θ_5, i.e.,

$$i_{bus} = \begin{cases} i_a + i_b, & \theta_1 < \theta \le \theta_2 \\ i_b, & \theta_2 < \theta \le \theta_3 \\ i_b + i_c, & \theta_3 < \theta \le \theta_4 \\ i_c, & \theta_4 < \theta \le \theta_5 \end{cases} \tag{4}$$

Clearly, only two excitation currents of adjacent phases are overlapped at most during running conditions, such as phases A and B, and phases B and C. According to the SRM operation principle, in order to obtain a positive phase torque, the excitation currents of phases A and C should never have any overlap, which is to say that phase C will not conduct when phase A is turned on. Similarly, the excitation currents of phases B and D will not have any overlap too. Therefore, one current sensor can be used to detect the excitation currents of

0278-0046 (c) 2017 IEEE. Personal use is permitted, but republication/redistribution requires IEEE permission. See http://www.ieee.org/publications_standards/publications/rights/index.html for more information.

This article has been accepted for publication in a future issue of this journal, but has not been fully edited. Content may change prior to final publication. Citation information: DOI 10.1109/TIE.2017.2772152, IEEE Transactions on Industrial Electronics

phases A and C. As shown in Fig. 3, the excitation currents of phases A and C in the turn-on regions (S_2 and S_6) are not overlapped. Therefore, by removing the demagnetization current of each phase, the excitation currents of phases A and C will not flow through this current sensor at the same time. According to the switching states S_2 and S_6, the excitation currents of phases A and C can be easily separated and obtained. Similarly, the excitation currents of phases B and D in the turn-on regions (S_4 and S_8) are also not overlapped. Therefore, they can be separated according to the switching states S_4 and S_8 if another current sensor is used to detect these two currents.

C. Proposed Current Measurement Technique with Split Dual Bus Line

Conventionally, individual hall-effect sensors are placed in each phase winding to measure the corresponding phase current for current regulation control in SRM drives, as shown in Fig. 4(a). The used sensors increase the cost and volume of the motor drive and decrease the system reliability. To reduce these hall-effect sensors, a single-sensor based phase current reconstruction scheme is put forward [34], as shown in Fig. 4(b). However, high-frequency pulses need to be injected into each phase to detect the phase currents from the bus line. This implementation will inevitably generate voltage penalty and additional switching loss. The voltage penalty leads to current distortion and affects the current measurement accuracy.

In order to solve the issues of pulse injection and voltage penalty, a new cost-effective current measurement scheme is proposed in this paper, by splitting dual bus line using two hall-effect sensors, without any pulse injection and voltage penalty, although the use of two current sensors instead of only one current sensor decreases the reliability, as shown in Fig. 4(c). The upper and lower bus lines are both split into two parts. In the split upper bus, the collectors of the upper switches of phases B and D are connected together through a current sensor to the dc link, which are divided from the other parts, while the other connections are the same. In the split lower bus, the emitters of the lower switches of phases A and B are connected together through another current sensor to the dc link, which are divided from the other parts, and the other connections are also the same. The two hall-effect current sensors are used to detect the upper and lower bus currents, respectively. In the developed converter topology, the two bus lines are split without additional change, and only two current sensors are utilized for current measurement on behalf of individual phase current sensors, which not only reduces the current sensors compared to traditional methods, but also presents a promising solution to the voltage penalty and current distortion, without pulse injection compared to the single-sensor scheme.

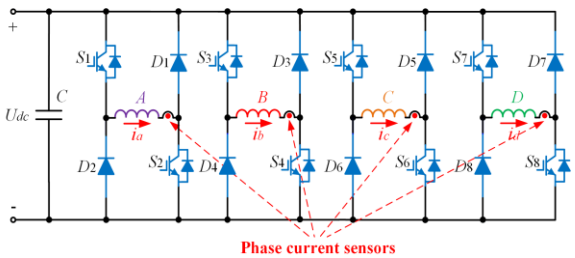

(a)

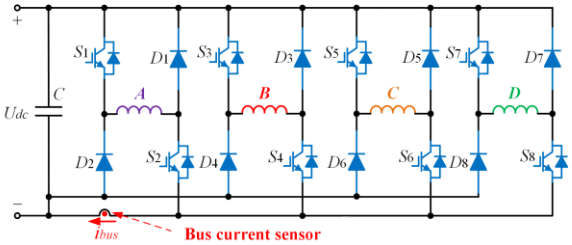

(b)

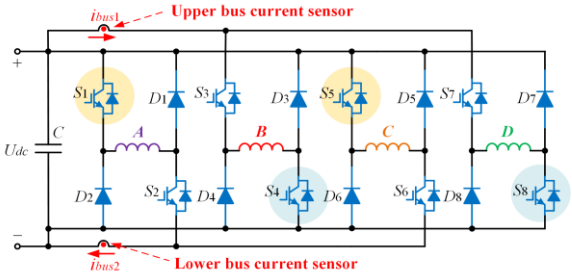

(c)

Fig. 4. Current measurement schemes. (a) Conventional current measurement scheme with individual hall-effect sensors. (b) Single-sensor based current measurement scheme [34]. (c) Proposed two-sensor based current measurement scheme with split dual bus line.

In Fig. 4(c), the demagnetization currents of phases A, B, C, and D will flow through diodes D_1 and D_2, D_3 and D_4, D_5 and D_6, and D_7 and D_8, respectively, to the dc link. Clearly, by splitting the dual bus line, the demagnetization currents, which are not needed for current regulation control, will not go through either of the two bus current sensors, making the phase current measurement and separation much easier.

In order to measure the phase currents during the whole turn-on regions, the switching functions are redesigned so that the upper switches of phases A and C, i.e., S_1 and S_5, act as the choppers for current regulation control and the lower switches S_2 and S_6 remain closed in the phase turn-on region; and the lower switches of phases B and D, i.e., S_4 and S_8, act as the choppers for current regulation control and the upper switches S_3 and S_7 remain closed in the phase turn-on region. Therefore, the operational modes of phases A and C are similar, and their currents can be measured by the lower bus current sensor. Also, the operational modes of phases B and D are similar, and their currents can be measured by the upper bus current sensor.

The working states of the new converter for two overlapped phases among phases A, B, and C in the turn-on regions, are illustrated in Fig. 5. Clearly, in phase A and B turn-on regions, even if phases A and B are in freewheeling or conduction states, phase A current always flows through the lower bus current sensor, and phase B current always flows through the upper bus current sensor, as shown in Fig. 5(a)~(d). Similarly, when phases B and C are both in the turn-on regions, phase B current always flows through the upper bus current sensor, and phase C current always flows through the lower bus current sensor, as shown in Fig. 5(e)~(h). Because phases A and C will never conduct at the same time, their currents in the lower bus sensor are directly separated, which can be done according to the corresponding turn-on regions. Therefore, there is only one phase current in each bus current sensor at each time.

0278-0046 (c) 2017 IEEE. Personal use is permitted, but republication/redistribution requires IEEE permission. See http://www.ieee.org/publications_standards/publications/rights/index.html for more information.

This article has been accepted for publication in a future issue of this journal, but has not been fully edited. Content may change prior to final publication. Citation information: DOI 10.1109/TIE.2017.2772152, IEEE Transactions on Industrial Electronics

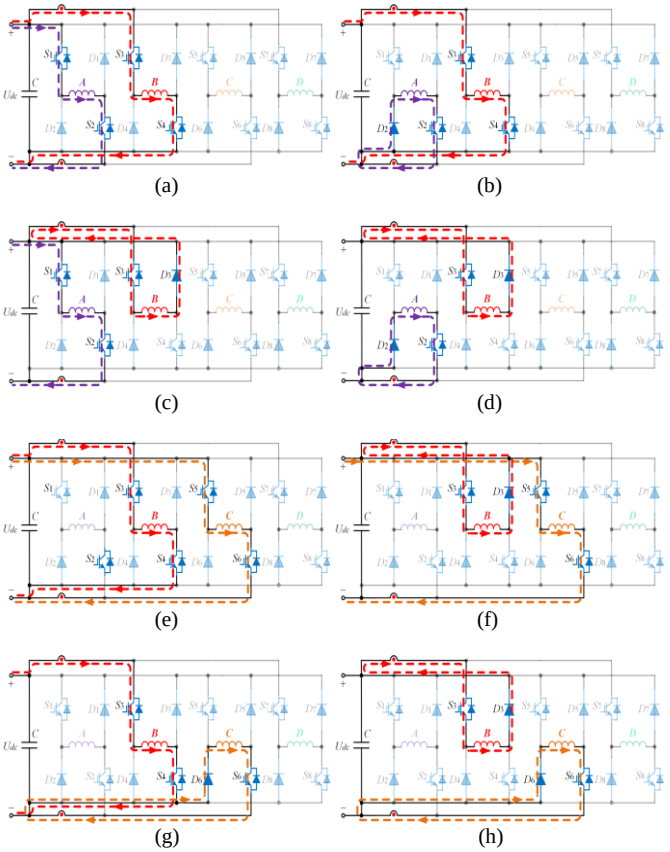

Fig. 5. Working states of the new converter topology. (a) Phases A and B conduction. (b) Phase A freewheeling and phase B conduction. (c) Phase A conduction and phase B freewheeling. (d) Phases A and B freewheeling. (e) Phases B and C conduction. (f) Phase B freewheeling and phase C conduction. (g) Phase B conduction and phase C freewheeling. (h) Phases B and C freewheeling.

In Region I (see Fig. 3), phases A and B are both in their turn-on regions. According to the analysis above, phase B current flows through the upper bus current sensor, and phase A current flows through the lower bus current sensor, as shown in Fig. 5(a)~(d). Therefore, the dual bus currents in Region I can be expressed as

$$\begin{cases} i_{bus1} = i_b \\ i_{bus2} = i_a \end{cases} \tag{5}$$

where i_{bus1} and i_{bus2} are the currents in upper and lower bus current sensors, respectively.

In Region II, phase B current still flows through the upper bus current sensor, and phase A is turned off. Phase A current will go through the two diodes D_1 and D_2 to the dc link, which will not go through either of the two bus current sensors. Thus, the dual bus currents in Region II can be expressed as

$$\begin{cases} i_{bus1} = i_b \\ i_{bus2} = 0 \end{cases} \tag{6}$$

Similarly, in Region III, phases B and C are both in their turn-on regions. Phase B current flows through the upper bus current sensor, and phase C current flows through the lower bus current sensor, as shown in Fig. 5(e)~(h). The dual bus currents in this region can be expressed as

$$\begin{cases} i_{bus1} = i_b \\ i_{bus2} = i_c \end{cases} \tag{7}$$

In Region IV, phase B is turned off and phase C is still in the turn-on region. Phase B current will go through the two diodes D_3 and D_4 to the dc link. There is no current in the upper bus current sensor, and the two bus currents are

$$\begin{cases} i_{bus1} = 0 \\ i_{bus2} = i_c \end{cases} \tag{8}$$

Clearly, each phase current can be directly measured by the dual bus current sensors in the corresponding turn-on region without additional switching actions.

The switching functions of the power switches in the converter are defined as

$$S_k = \begin{cases} 1, & \text{Power switch is on} \\ 0, & \text{Power switch is off} \end{cases}, \quad k = 2,3,6,7 \tag{9}$$

where S_2, S_3, S_6, and S_7 are the drive signals for the non-chopping switches.

The dual bus currents can be expressed in terms of the phase currents and switching functions as

$$i_{bus1} = i_b \cdot S_3 + i_d \cdot S_7 \tag{10}$$

$$i_{bus2} = i_a \cdot S_2 + i_c \cdot S_6 \tag{11}$$

The relationship between the dual bus currents and switching states in a four-phase conduction cycle is presented in Table I. Clearly, phase B and D currents can be measured by the upper bus current sensor, and phase A and C currents can be measured by the lower bus current sensor. Both of the two bus currents only contain one phase current at most in each switching state.

TABLE I
RELATIONSHIP BETWEEN DUAL BUS CURRENTS AND SWITCHING STATES

S_2	S_3	S_6	S_7	i_{bus1}	i_{bus2}
1	0	0	0	0	i_a
1	1	0	0	i_b	i_a
0	1	0	0	i_b	0
0	1	1	0	i_b	i_c
0	0	1	0	0	i_c
0	0	1	1	i_d	i_c
0	0	0	1	i_d	0
1	0	0	1	i_d	i_a

Hence, according to the relationship between the dual bus currents and switching functions, the excitation currents of phases A, B, C, and D can be fully obtained by (12) for control.

$$\begin{cases} i_a' = i_{bus2} \cdot S_2 \\ i_b' = i_{bus1} \cdot S_3 \\ i_c' = i_{bus2} \cdot S_6 \\ i_d' = i_{bus1} \cdot S_7 \end{cases} \tag{12}$$

III. SIMULATION RESULTS

A simulation model is set up in Matlab/Simulink to validate the feasibility of the proposed scheme, as shown in Fig. 6. A 150 W four-phase 8/6-pole SRM is employed for the simulation, and the main parameters of the motor are presented in Table II.

0278-0046 (c) 2017 IEEE. Personal use is permitted, but republication/redistribution requires IEEE permission. See http://www.ieee.org/publications_standards/publications/rights/index.html for more information.

This article has been accepted for publication in a future issue of this journal, but has not been fully edited. Content may change prior to final publication. Citation information: DOI 10.1109/TIE.2017.2772152, IEEE Transactions on Industrial Electronics

The proposed converter is built by using the IGBT and diode models from SimPowerSystems. The split dual bus line is achieved by connecting the upper switches of phases B and D in the upper bus, and the lower switches of phases A and C in the lower bus. As shown in Fig. 6(a), the four phase currents are measured by detecting the dual bus currents and used for current regulation control. The current hysteresis controller is employed to generate the switching signals during the turn-on regions. The rotor position for each phase is calculated according to the integral of the angular velocity. As shown in Fig. 6(b), two look-up tables including flux-current-position (ψ-i-θ) and torque-current-position (T-i-θ) characteristics are used to build the SRM model, which are obtained by the numerical electromagnetic analysis in Ansoft software. The real-time phase current and torque are output from the two look-up tables, according to the voltage on the phase winding and rotor position.

TABLE II
MOTOR PARAMETERS

Parameters	Value
Phase number	4
Stator/rotor poles	8/6
Rated power (W)	150
Rated voltage (V)	132
Rated current (A)	1.0
Rated torque (N·m)	0.95
Rated speed (r/min)	1500
Phase resistor (Ω)	9
Minimum phase inductance (mH)	28.65
Maximum phase inductance (mH)	226.03
Rotor outer diameter (mm)	54
Rotor inner diameter (mm)	22
Stator outer diameter (mm)	102
Stator inner diameter (mm)	54.5
Stack length (mm)	58
Stator arc angle (deg)	21
Rotor arc angle (deg)	24

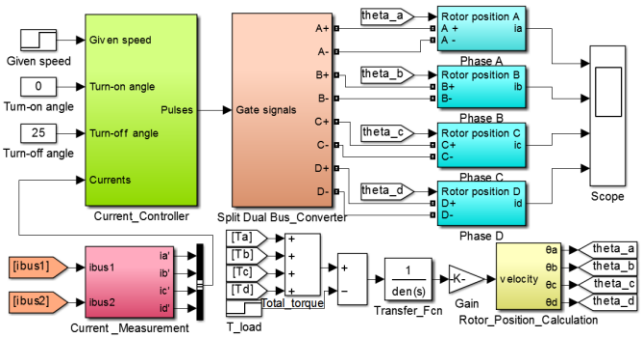

(a)

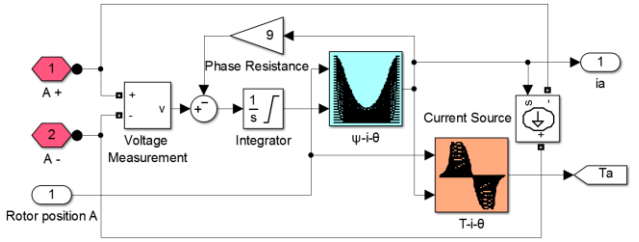

(b)

Fig. 6. Simulation model of the SRM system. (a) System model. (b) SRM model for one phase.

Fig. 7 illustrates the simulation results under low-speed operation at 300 r/min. The turn-on and turn-off angles are set to 0° and 25°, respectively, and the current hysteresis width is set to 0.08 A. As shown in Fig. 7(a), the upper switches of phases A and C, i.e., S_1 and S_5, are used as the choppers, while the lower switches of phases B and D, i.e., S_4 and S_8 act as the choppers. Fig. 7(b) presents the dual bus currents and individual phase currents waveforms. Clearly, the phase currents do not overlap in both of the upper and lower bus lines, and the shape of the dual bus current is the same as the phase currents in their turn-on regions. The relationship between the bus current, phase currents, and drive signals is presented in Fig. 7(c) and (d). It can be seen that the upper bus current is the sum of phase B and D currents in their turn-on regions. Therefore, phase B and D currents can be directly obtained according to the upper bus current and switching signals related to the turn-on regions of phases B and D. Similarly, the lower bus current is the sum of phase A and C currents in their turn-on regions. Thus, phase A and C currents can also be directly acquired according to the lower bus current and switching signals related to the turn-on regions of phases A and C.

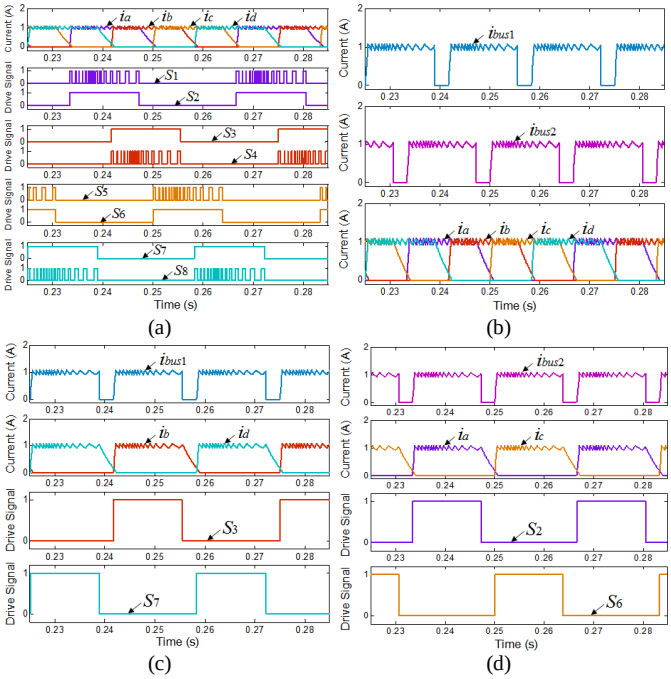

(a) (b) (c) (d)

Fig. 7. Simulation results for low-speed operation. (a) Phase currents and drive signals. (b) Dual bus currents and phase currents. (c) Upper bus current, phase B and D currents, and drive signals. (d) Lower bus current, phase A and C currents, and drive signals.

When the motor operates at high speed, the chopping cycles contained in a phase conduction period would disappear. Fig. 8 shows the simulation results at 1500 r/min, and the turn-on and turn-off angles are set to 0° and 20°, respectively. Because there is no chopping actions for the switches in this condition, the drive signals for the upper and lower switches in each phase are the same, as shown in Fig. 8(a). The same as low-speed operation conditions, the upper and lower bus currents contain all the phase current information in the turn-on regions, where the phase currents do not overlap, as shown in Fig. 8(b). Clearly, the upper bus current is the sum of phase B and D currents in

0278-0046 (c) 2017 IEEE. Personal use is permitted, but republication/redistribution requires IEEE permission. See http://www.ieee.org/publications_standards/publications/rights/index.html for more information.

This article has been accepted for publication in a future issue of this journal, but has not been fully edited. Content may change prior to final publication. Citation information: DOI 10.1109/TIE.2017.2772152, IEEE Transactions on Industrial Electronics

their turn-on regions, and the phase B and D currents are naturally separated in the upper bus line due to non-overlapping, as shown in Fig. 8(c). The lower bus current is the sum of phase A and C currents in their turn-on regions, and the phase A and C currents are also naturally separated in the lower bus line due to non-overlapping, as shown in Fig. 8(d). Therefore, all four phase currents can be directly calculated according to the dual bus currents and switching signals related to the turn-on regions.

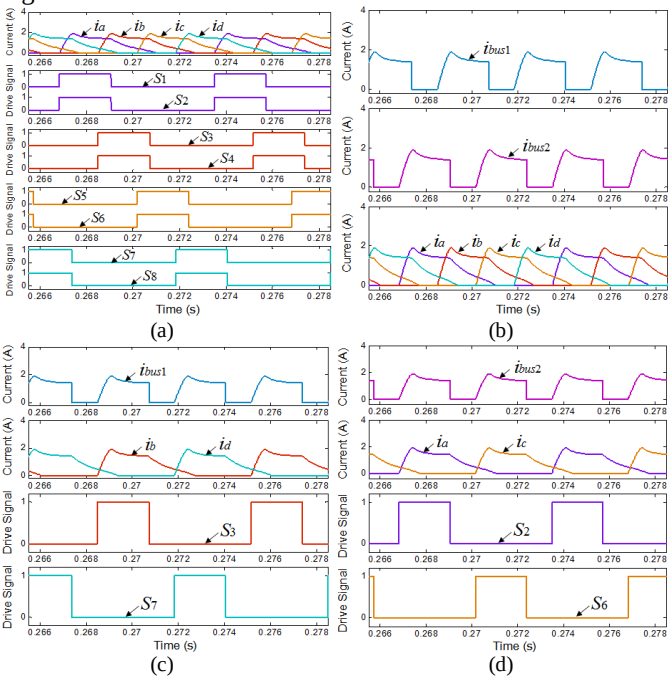

Fig. 8. Simulation results for high-speed operation. (a) Phase currents and drive signals. (b) Dual bus currents and phase currents. (c) Upper bus current, phase B and D currents, and drive signals. (d) Lower bus current, phase A and C currents, and drive signals.

IV. Experimental Verification

In order to verify the proposed current measurement and control technique based on experiments, a 150 W four-phase 8/6 SRM prototype is employed to build an experimental test-rig, and the parameters of the test motor are the same as the simulation. The photo and schematic diagram of the motor system are illustrated in Fig. 9. As shown in Fig. 9(a), a dSPACE-DS1006 platform is employed as the main controller to implement the proposed scheme. In the motor test bed, a Parker AC servomotor acts as the load, which is controlled by an integrated load controller inside the cabinet. A high-precision torque sensor is installed between the SRM and load motor to detect the instantaneous output torque. A 2500-line incremental encoder is installed on the motor frame to detect the rotor position. A dc power supply is utilized to drive the motor system. A multi-channel isolated oscilloscope is used to observe the waveforms of the currents and switching signals. As shown in Fig. 9(b), the new converter is formed by splitting both the upper and lower bus lines, and two hall-effect sensors (LA-55P) are used in the dual bus, respectively, to detect the corresponding currents. The currents are sampled by two 14-bit A/D conversion channels for closed-loop current regulation control.

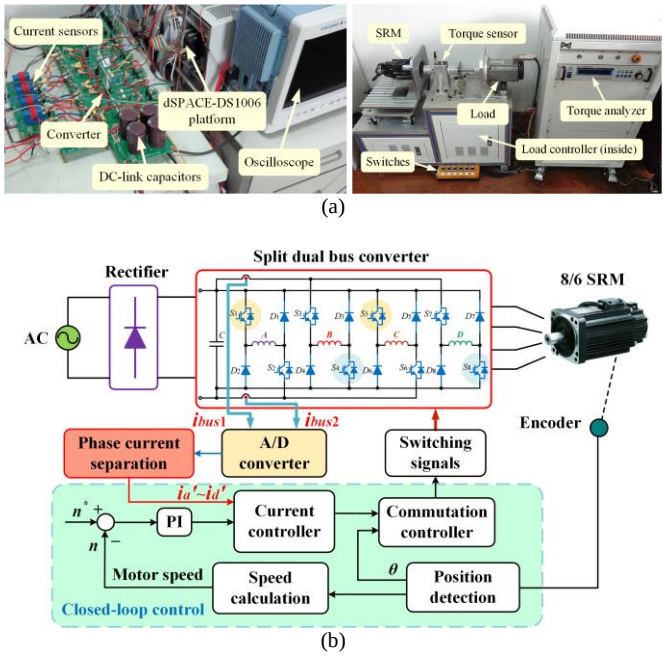

Fig. 9. Experimental system of the proposed SRM drive. (a) Photo of the experimental setup. (b) Schematic diagram.

Fig. 10 presents the experimental results in low-speed operation at 300 r/min. The turn-on and turn-off angle are set to 0° and 25°, respectively, and the load is set to 0.95 N·m, which are the same as the simulation. As shown in Fig. 10(a), the upper switches of phases A and C are used as the choppers, while the lower switches of phases B and D are employed as the choppers, due to the new converter configuration design. The waveforms of the dual bus currents and individual phase currents are given in Fig. 10(b) for comparison. Clearly, the two bus currents have included the four phase currents information in the turn-on regions. Fig. 10(c) and (d) show the detailed relationship between the dual bus currents, phase currents and switching signals with respect to the turn-on regions. The upper bus current contains the phase B current in its turn-on region and phase D current in its turn-on region, as shown in Fig.10 (c); the lower bus current contains both the phase A and phase C currents in their turn-on regions, as shown in Fig.10 (d). The experimental results in high-speed operation at 1500 r/min are shown in Fig.11, where the turn-on and turn-off angles are set to 0° and 20°, respectively. The dual bus currents still cover all the phase current information in the turn-on regions. Therefore, the four phase currents can be directly obtained according to the dual bus currents and switching signals no matter in low- or high-speed operation, which can be used for current regulation control. The experimental results in Figs. 10 and 11 show good consistency with the simulation results.

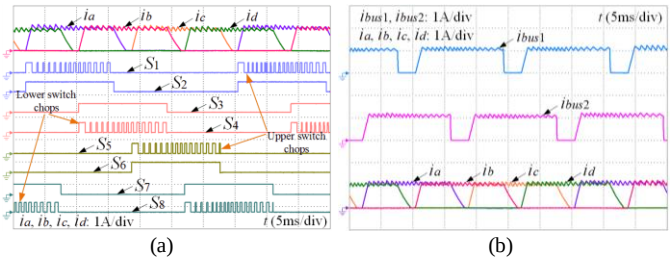

0278-0046 (c) 2017 IEEE. Personal use is permitted, but republication/redistribution requires IEEE permission. See http://www.ieee.org/publications_standards/publications/rights/index.html for more information.

This article has been accepted for publication in a future issue of this journal, but has not been fully edited. Content may change prior to final publication. Citation information: DOI 10.1109/TIE.2017.2772152, IEEE Transactions on Industrial Electronics

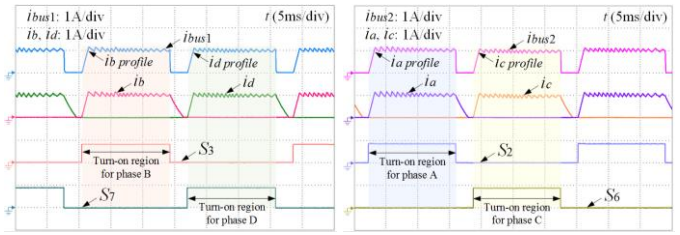

(c) (d)

Fig. 10. Experimental results for low-speed operation. (a) Phase currents and drive signals. (b) Dual bus currents and phase currents. (c) Upper bus current, phase B and D currents, and drive signals. (d) Lower bus current, phase A and C currents, and drive signals.

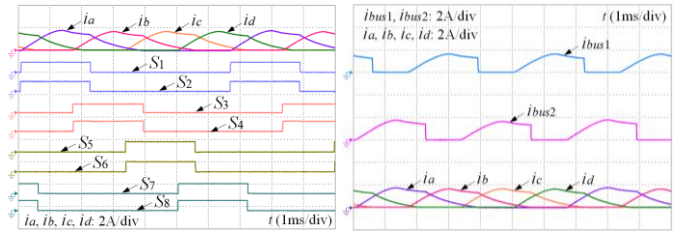

(a) (b)

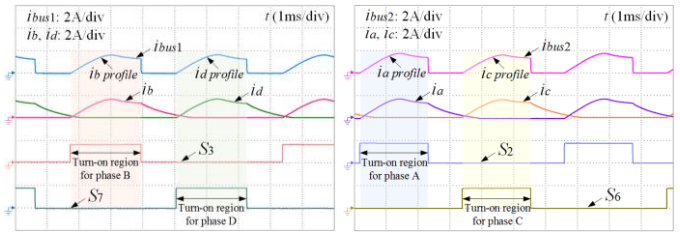

(c) (d)

Fig. 11. Experimental results for high-speed operation. (a) Phase currents and drive signals. (b) Dual bus currents and phase currents. (c) Upper bus current, phase B and D currents, and drive signals. (d) Lower bus current, phase A and C currents, and drive signals.

Fig. 12 gives a current comparison between the two bus currents and phase currents, where i_a', i_b', i_c', and i_d' are the phase currents in turn-on regions. Clearly, the upper bus current tracks well with the signals of the phase B and phase D currents multiplying their corresponding switching signals, respectively, which can be directly used for phase B and D control. Similarly, the lower bus current tracks well with the signals of the phase A and phase C currents multiplying their corresponding switching signals, respectively, which can be directly used for phase A and C control. Therefore, the current control can be achieved by measuring the dual bus currents without using individual phase sensors. Additionally, there is no need to reselect the hall-effect sensors with larger measuring ranges, because the phase currents are not overlapped in both the upper and lower bus sensors.

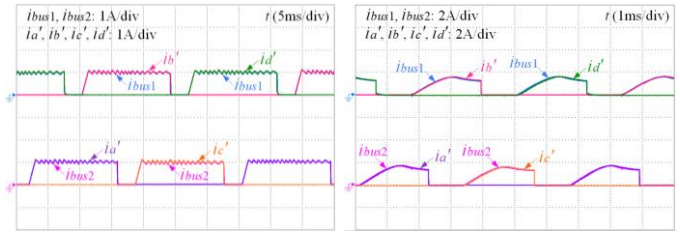

(a) (b)

Fig. 12. Comparison between dual bus currents and phase currents in turn-on regions. (a) 300 r/min. (b) 1500 r/min.

In order to investigate the control performance in a closed-loop system by using the new scheme, the transient response to step changes including speed regulation, load variation, and angle modulation, are shown in Fig. 13. When the speed increases from 300 to 600 r/min and from 600 to 1000 r/min, the instantaneous speed tracks the given reference well, as shown in Fig. 13(a). When the load increases from no-load to 0.95 N·m and from 0.95 to 1.8 N·m, the speed is rapidly stabilized at the given value within 200 ms, as shown in Fig. 13(b). In terms of the angle modulations, the speed can still be easily controlled when the turn-on angle changes from −4° to 0° and from 0° to 4°, and when the turn-off angle changes from 20° to 25° and from 25° to 28°, as shown in Fig. 13(c) and (d), respectively, confirming a good robustness to fast transients.

Fig. 14 presents the comparison on system efficiency and ripple torque between the traditional individual-sensor scheme and proposed split-dual-bus scheme. For low-power SRMs, their system efficiency is relatively low [36]-[38]. However, it is clear that there is no efficiency decrease and torque ripple increase, by using the proposed current sensing scheme. Compared to the single-sensor scheme [33], [34], there is no need to inject any pulses into the drive signals to detect the phase currents, which provides a promising solution to voltage penalty, current distortion and lower efficiency inherent in other methods.

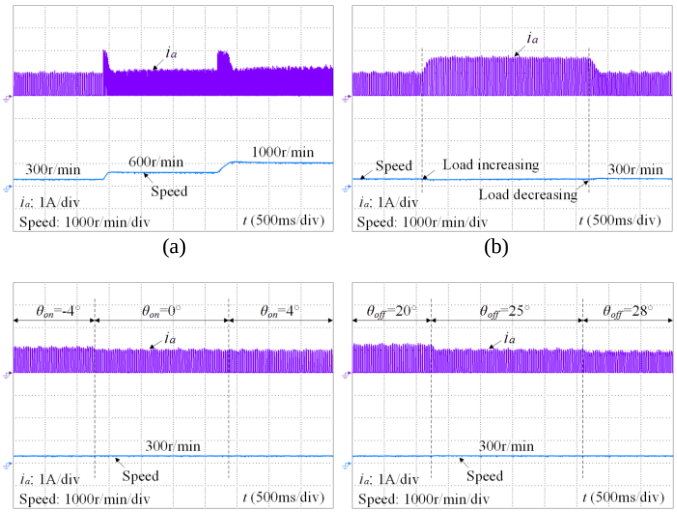

(a) (b) (c) (d)

Fig. 13. Transient response to step changes. (a) Speed regulation. (b) Load variation. (c) Turn-on angle modulation. (d) Turn-off angle modulation.

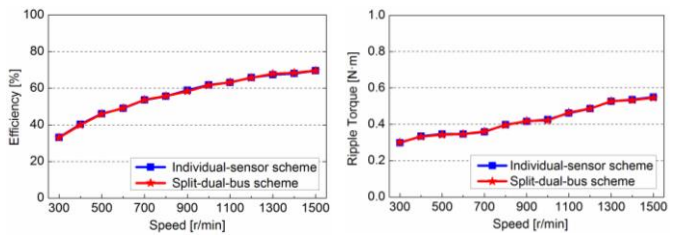

(a) (b)

Fig. 14. Comparison on efficiency and torque ripple between the individual-sensor scheme and split-dual-bus scheme. (a) Efficiency. (b) Ripple torque.

0278-0046 (c) 2017 IEEE. Personal use is permitted, but republication/redistribution requires IEEE permission. See http://www.ieee.org/publications_standards/publications/rights/index.html for more information.

This article has been accepted for publication in a future issue of this journal, but has not been fully edited. Content may change prior to final publication. Citation information: DOI 10.1109/TIE.2017.2772152, IEEE Transactions on Industrial Electronics

It should be noted that a low-power SRM is employed for proof-of-concept. Therefore, this technology can be used for low power applications, such as home appliances, micro EVs, low-power electric sightseeing cars, etc. However, the operational modes of the converter (i.e., excitation and demagnetization) and the current paths through the dual bus line will not be changed with higher power levels. The proposed SRM drive shows good scalability to build up to high-voltage and high-power systems with suitable modifications if required. Furthermore, in high-performance and safety-critical applications, the proposed scheme can also provide a simple, reliable, and cost-efficient fault-tolerance method for individual phase sensor faults.

V. Conclusion

This paper proposes a simple and cost-effective current measurement technique for four-phase SRM control, by splitting the dual bus line of the converter, without any pulse injection and voltage penalty generation. The upper and lower bus lines are both split into two parts, and two current sensors are utilized in the split dual bus lines, respectively, to detect the upper and lower bus currents, where the phase currents can be directly obtained according to the switching functions. With this technique, current control strategies can be implemented by using the currents detected from the dual bus line. The main contributions of this paper are as follows:

(1) Compared to the individual-sensor scheme, the hall-effect current sensors are reduced and only two sensors are utilized in the dual bus line without any additional circuits, making the product more compact and reliable.

(2) Compared to the single-sensor based strategy, there is no need to inject any pulses into drive signals, which will not generate any voltage penalty leading to current distortion and cause any additional switching loss. In terms of the reliability, although one more sensor is used, there is no need to inject additional pulses into drive signals, which will also increase the system reliability and efficiency. In terms of the complexity, the currents do not need to be sampled at specific sampling instants under pulse injection. Also, there is no need to reselect the sensors with larger measuring ranges, because the currents flowing through the dual sensors are not overlapped. Therefore, the new scheme is really simple to implement and the complexity can be reduced compared to the single-sensor scheme, which will also improve the current measurement accuracy and system performance.

(3) In high performance and safety critical applications, the proposed scheme can also provide a simple, reliable and cost-efficient fault-tolerant method for current sensor faults, even if fault occurs in one or multiple sensors.

References

[1] S. S. Williamson, A. K. Rathore, F. Musavi, "Industrial electronics for electric transportation: current state-of-the-art and future challenges," *IEEE Trans. Ind. Electron.*, vol. 62, DOI 10.1109/TIE.2015.2409052, no. 5, pp. 3021 - 3032, May. 2015.

[2] A. Choudhury, P. Pillay, and S. S. Williamson, "Modified dc-bus voltage-balancing algorithm based three-level neutral-point-clamped IPMSM drive for electric vehicle applications," *IEEE Trans. Ind. Electron.*, vol. 63, DOI 10.1109/TIE.2015.2478392, no. 2, pp. 761-772, Feb. 2016.

[3] O. C. Onar, J. Kobayashi, and A. Khaligh, "A fully directional universal power electronic interface for EV, HEV, and PHEV Applications," *IEEE Trans. Power Electron.*, vol. 28, DOI 10.1109/TPEL.2012.2236106, no. 12, pp. 5489-5498, Dec. 2013.

[4] G. Zhang, W. Hua, M. Cheng, and J. Liao, "Design and comparison of two six-phase hybrid-excited flux-switching machines for EV/HEV applications," *IEEE Trans. Ind. Electron.*, vol. 63, DOI 10.1109/TIE.2015.2447501, no. 1, pp. 481-493, Jan. 2016.

[5] S. Rivera and B. Wu, "Electric vehicle charging station with an energy storage stage for split-dc bus voltage balancing," *IEEE Trans. Power Electron.*, vol. 32, DOI 10.1109/TPEL.2016.2568039, no. 3, pp. 2376-2386, Mar. 2017.

[6] V. Ruuskanen, J. Nerg, M. Rilla, and J. Pyrhonen, "Iron loss analysis of the permanent-magnet synchronous machine based on finite-element analysis over the electrical vehicle drive cycle," *IEEE Trans. Ind. Electron.*, vol. 63, DOI 10.1109/TIE.2016.2549005, no. 7, pp. 4129-4136, Jul. 2016.

[7] Y. Miyama, M. Hazeyama, S. Hanioka, N. Watanabe, A. Daikoku, and M. Inoue, "PWM carrier harmonic iron loss reduction technique of permanent-magnet motors for electric vehicles," *IEEE Trans. Ind. Appl.*, vol. 52, DOI 10.1109/TIA.2016.2533598, no. 4, pp. 2865-2871, Jul./Aug. 2016.

[8] X. Liu, H. Chen, J. Zhao, and A. Belahcen, "Research on the performances and parameters of interior PMSM used for electric vehicles," *IEEE Trans. Ind. Electron.*, vol. 63, DOI 10.1109/TIE.2016.2524415, no. 6, pp. 3533-3545, Jun. 2016.

[9] C. H. T. Lee, K. T. Chau, and C. Liu, "Design and analysis of an electronic-geared magnetless machine for electric vehicles," *IEEE Trans. Ind. Electron.*, vol. 63, DOI 10.1109/TIE.2016.2582793, no. 11, pp. 6705-6714, Nov. 2016.

[10] N. Bianchi, S. Bolognani, E. Carraro, M. Castiello, and E. Fornasiero, "Electric vehicle traction based on synchronous reluctance motors," *IEEE Trans. Ind. Appl.*, vol. 52, DOI 10.1109/TIA.2016.2599850, no. 6, pp. 4762-4769, Nov./Dec. 2016.

[11] I. Boldea, L. N. Tutelea, L. Parsa, and D. Dorrell, "Automotive electric propulsion systems with reduced or no permanent magnets: an overview," *IEEE Trans. Ind. Electron.*, vol. 61, DOI 10.1109/TIE.2014.2301754, no. 10, pp. 5696-5711, Oct. 2014.

[12] J. Santiago, H. Bernhoff, B. Ekergard, S. Eriksson, S. Ferhatovic, R. Waters, and M. Leijon, "Electrical motor drivelines in commercial all-electric vehicles: a review," *IEEE Trans. Veh. Technol.*, vol. 61, DOI 10.1109/TVT.2011.2177873, no. 2, pp. 475-484, Feb. 2012.

[13] J. Kim and R. Krishnan, "Novel two-switch-based switched reluctance motor drive for low-cost high-volume applications," *IEEE Trans. Ind. Appl.*, vol. 45, DOI 10.1109/TIA.2009.2023568, no. 4, pp. 1241–1248, Jul./Aug. 2009.

[14] Y. Kano, T. Kosaka, and N. Matsui, "Optimum design approach for a two-phase switched reluctance compressor drive," *IEEE Trans. Ind. Appl.*, vol. 46, DOI 10.1109/TIA.2010.2045212, no. 3, pp. 955–964, May/Jun. 2010.

[15] E. Bostanci, M. Moallem, A. Parsapour, and B. Fahimi, "Opportunities and challenges of switched reluctance motor drives for electric propulsion: a comparative study," *IEEE Trans. Transport. Electrific.*, vol. 3, DOI 10.1109/TTE.2017.2649883, no. 1, pp. 58-75, Mar. 2017.

[16] A. Chiba, K. Kiyota, N. Hoshi, M. Takemoto, and S. Ogasawara, "Development of a rare-earth-free SR motor with high torque density for hybrid vehicles," *IEEE Trans. Energy Convers.*, vol. 30, DOI 10.1109/TEC.2014.2343962, no. 1, pp. 175–182, Mar. 2015.

[17] K. Kiyota, T. Kakishima, A. Chiba, and M. A. Rahman, "Cylindrical rotor design for acoustic noise and windage loss reduction in switched reluctance motor for HEV applications," *IEEE Trans. Ind. Appl.*, vol. 52, DOI 10.1109/TIA.2015.2466558, no. 1, pp. 154-162, Jan./Feb.2016.

[18] S. Song, Z. Xia, Z. Zhang, and W. Liu, "Control performance analysis and improvement of a modular power converter for three-phase SRM with Y-connected windings and neutral line," *IEEE Trans. Ind. Electron.*, vol. 63, DOI 10.1109/TIE.2016.2577543, no. 10, pp. 6020-6030, Oct. 2016.

[19] C. Gan, J. Wu, Y. Hu, S. Yang, W. Cao, and J. M. Guerrero, "New integrated multilevel converter for switched reluctance motor drives in plug-in hybrid electric vehicles with flexible energy conversion," *IEEE Trans. Power Electron.*, vol. 32, no. 5, pp. 3754-3766, May 2017.

[20] W. Ding, Y. Hu, and L. Wu, "Investigation and experimental test of fault-tolerant operation of a mutually coupled dual three-phase SRM drive under faulty conditions," *IEEE Trans. Power Electron.*, vol. 30, DOI 10.1109/TPEL.2015.2389258, no. 12, pp. 6857-6872, Dec. 2015.

0278-0046 (c) 2017 IEEE. Personal use is permitted, but republication/redistribution requires IEEE permission. See http://www.ieee.org/publications_standards/publications/rights/index.html for more information.

This article has been accepted for publication in a future issue of this journal, but has not been fully edited. Content may change prior to final publication. Citation information: DOI 10.1109/TIE.2017.2772152, IEEE Transactions on Industrial Electronics

[21] J. Ye, B. Bilgin, and A. Emadi, "An extended-speed low-ripple torque control of switched reluctance motor drives," *IEEE Trans. Power Electron.*, vol. 30, DOI 10.1109/TPEL.2014.2316272, no. 3, pp. 1457-1470, Mar. 2015.

[22] B. Bilgin, A. Emadi, and M. Krishnamurthy, "Comprehensive evaluation of the dynamic performance of a 6/10 SRM for traction application in PHEVs," *IEEE Trans. Ind. Electron.*, vol. 60, DOI 10.1109/TIE.2012.2196015, no. 7, pp. 2564–2575, Jul. 2013.

[23] K. M. Rahman, B. Fahimi, G. Suresh, A. V. Rajarathnam, and M. Ehsani, "Advantages of switched reluctance motor applications to EV and HEV: design and control issues," *IEEE Trans. Ind. Appl.*, vol. 36, DOI 10.1109/28.821805, no. 1, pp. 111-121, Jan./Feb. 2000.

[24] H. Chen, H. Yang, Y. Chen, and H. H. C. Iu, "Reliability assessment of the switched reluctance motor drive under single switch chopping strategy," *IEEE Trans. Power Electron.*, vol. 31, DOI 10.1109/TPEL.2015.2429557, no. 3, pp. 2395-2408, Mar. 2016.

[25] F. Yi and W. Cai, "Modeling, control, and seamless transition of the bidirectional battery-driven switched reluctance motor/generator drive based on integrated multiport power converter for electric vehicle applications," *IEEE Trans. Power Electron.*, vol. 31, DOI 10.1109/TPEL.2015.2510286, no. 10, pp. 7099-7111, Oct. 2016.

[26] D. P. Marcetic and E. M. Adzic, "Improved three-phase current reconstruction for induction motor drives with dc-link shunt," *IEEE Trans. Ind. Electron.*, vol. 57, DOI 10.1109/TIE.2009.2035456, no. 7, pp. 2454-2462, Jul. 2010.

[27] H. Lu, X. Cheng, W. Qu, S. Sheng, Y. Li, and Z. Wang, "A three-phase current reconstruction technique using single dc current sensor based on TSPWM," *IEEE Trans. Power Electron.*, vol. 29, DOI 10.1109/TPEL.2013.2266408, no. 3, pp. 1542-1550, Mar. 2014.

[28] Y. Gu, F. Ni, D. Yang, and H. Liu, "Switching-state phase shift method for three-phase-current reconstruction with a single dc-link current sensor," *IEEE Trans. Ind. Electron.*, vol. 58, DOI 10.1109/TIE.2011.2123854, no. 11, pp. 5186-5194, Nov. 2011.

[29] Y. S. Lai, Y. K. Lin, and C. W. Chen, "New hybrid pulsewidth modulation technique to reduce current distortion and extend current reconstruction range for a three-phase inverter using only dc-link sensor," *IEEE Trans. Power Electron.*, vol. 28, DOI 10.1109/TPEL.2012.2207406, no. 3, pp. 1331-1337, Mar. 2013.

[30] Y. Xu, H. Yan, J. Zou, B. Wang, and Y. Li, "Zero voltage vector sampling method for PMSM three-phase current reconstruction using single current sensor," *IEEE Trans. Power Electron.*, vol. 32, DOI 10.1109/TPEL.2016.2588141, no. 5, pp. 3797-3807, May 2017.

[31] X. Li, S. Dusmez, B. Akin, and K. Rajashekara, "A new SVPWM for the phase current reconstruction of three-phase three-level T-type converters," *IEEE Trans. Power Electron.*, vol. 31, DOI 10.1109/TPEL.2015.2440421, no. 3, pp. 2627-2637, Mar. 2016.

[32] H. Shin and J. I. Ha, "Phase current reconstructions from dc-link currents in three-phase three-level PWM inverters," *IEEE Trans. Power Electron.*, vol. 29, DOI 10.1109/TPEL.2013.2257866, no. 2, pp. 582-593, Feb. 2014.

[33] P. C. Kjaer and G. G. Lopez, "Single-sensor current regulation in switched reluctance motor drives," *IEEE Trans. Ind. Appl.*, vol. 34, DOI 10.1109/28.673713, no. 3, pp. 444–451, May/Jun. 1998

[34] C. Gan, J. Wu, S. Yang, and Y. Hu, "Phase current reconstruction of switched reluctance motors from dc-link current under double high-frequency pulses injection," *IEEE Trans. Ind. Electron.*, vol. 62, DOI 10.1109/TIE.2014.2364153, no. 5, pp. 3265-3276, May 2015.

[35] C. Gan, J. Wu, Y. Hu, S. Yang, W. Cao, and J. L. Kirtley, "Online sensorless position estimation for switched reluctance motors using one current sensor," *IEEE Trans. Power Electron.*, vol. 31, DOI 10.1109/TPEL.2015.2505706, no. 10, pp. 7248-7263, Oct. 2016.

[36] K. M. Rahman and S. E. Schulz, "Design of high-efficiency and high-torque-density switched reluctance motor for vehicle propulsion," *IEEE Trans. Ind. Appl.*, vol. 38, DOI 10.1109/TIA.2002.805571, no. 6, pp. 1500–1507, Nov./Dec. 2002.

[37] D. H. Lee, J. Liang, Z. G. Lee, and J. W. Ahn, "A simple nonlinear logical torque sharing function for low-torque ripple SR drive," *IEEE Trans. Ind. Electron.*, vol. 56, DOI 10.1109/TIE.2009.2024661, no. 8, pp. 3021–3028, Aug. 2009.

[38] H. Y. Yang, Y. C. Lim, and H. C. Kim, "Acoustic noise/vibration reduction of a single-phase SRM using skewed stator and rotor," *IEEE Trans. Ind. Electron.*, vol. 60, DOI 10.1109/TIE.2012.2217715, no. 10, pp. 4292–4300, Oct. 2013.

Chun Gan (S'14–M'16) received the B.S. and M.S. degrees in power electronics and motor drives from China University of Mining and Technology, Jiangsu, China, in 2009 and 2012, respectively, and the Ph.D. degree in power electronics and motor drives from Zhejiang University, Hangzhou, China, in 2016.

He is currently a Research Associate with the Department of Electrical Engineering and Computer Science, The University of Tennessee, Knoxville, TN, USA. He is also a member of the U.S. Energy/National Science Foundation cofunded Engineering Research Center CURENT. He has published more than 40 technical papers in leading journals and conference proceedings, and authored one book chapter. He has ten issued/published invention patents. His research interests include high-efficiency power converters, electric vehicles, electrical motor drives, electrical motor design, continuous variable series reactors, high-voltage direct current transmission, and microgrids.

Dr. Gan received the 2015 Top Ten Excellent Scholar Award, the 2016 Excellent Ph.D. Graduate Award, the 2015 Ph.D. National Scholarship, the 2015 Wang Guosong Scholarship, and the 2014 and 2015 Outstanding Ph.D. Candidate Awards in Zhejiang University.

Qingguo Sun received the B.S. degree in Electrical Engineering from Qingdao University, Shandong, China, in 2014. He is currently working toward Ph.D. degree at the College of Electrical Engineering, Zhejiang University, Hangzhou, China.

His research interests include motor design and control in switched reluctance motor, particularly for the optimization of the torque ripple and efficiency of the motor system.

Nan Jin (M'16) received the B.S. and M.S. degrees in electrical engineering from Zhengzhou University of Light Industry, Zhengzhou, China, in 2003 and 2007, respectively, and Ph.D. degree in power electronics and electrical drives from Shanghai Jiao Tong University, Shanghai, China, in 2012

He is an associate professor in Zhengzhou University of Light Industry, Zhengzhou, China. He is currently a visiting professor with the Department of Electrical Engineering and Computer Science, The University of Tennessee, Knoxville, TN, USA. He has published more than 30 technical papers in journals and conference proceedings, two books and hold 8 Chinese patents. His research interests include model predictive control method for power converter, fault diagnosis and tolerant control of power electronics system.

Leon M. Tolbert (S'88–M'91–SM'98–F'13) received the bachelor's, M.S., and Ph.D. degrees in electrical engineering from the Georgia Institute of Technology, Atlanta, GA, USA, in 1989, 1991, and 1999, respectively.

He was with Oak Ridge National Laboratory, Oak Ridge, TN, from 1991 until 1999. He was appointed as an Assistant Professor in the Department of Electrical and Computer Engineering, The University of Tennessee, Knoxville, TN, USA, in 1999. He is currently the Min H. Kao Professor and the Department Head in Electrical Engineering and Computer Science, The University of Tennessee. He is a founding member of the National Science Foundation/Department of Energy Research Center, Center for Ultra-Wide-Area Resilient Electric Energy Transmission Networks. He is also a part-time Senior Research Engineer in the Power Electronics and Electric Machinery Research Center, Oak Ridge National Laboratory. In 2010, he was a Visiting Professor with Zhejiang University, Hangzhou, China.

0278-0046 (c) 2017 IEEE. Personal use is permitted, but republication/redistribution requires IEEE permission. See http://www.ieee.org/publications_standards/publications/rights/index.html for more information.

This article has been accepted for publication in a future issue of this journal, but has not been fully edited. Content may change prior to final publication. Citation information: DOI 10.1109/TIE.2017.2772152, IEEE Transactions on Industrial Electronics

Prof. Tolbert is a Registered Professional Engineer in the State of Tennessee. He received the 2001 IEEE Industry Applications Society Outstanding Young Member Award, and six Prize Paper Awards from the IEEE Industry Applications Society and the IEEE Power Electronics Society. From 2003 to 2006, he was the Chairman of the Education Activities Committee of the IEEE Power Electronics Society and an Associate Editor for the IEEE POWER ELECTRONICS LETTERS. He was an Associate Editor for the IEEE TRANSACTIONS ON POWER ELECTRONICS from 2007 to 2013. He was elected to serve as a Member-At-Large to the IEEE Power Electronics Society Advisory Committee for 2010–2012, the Chair of the PELS Membership Committee from 2011 to 2012, and a member of the PELS Nominations Committee from 2012 to 2014. He is currently the Paper Review Chair for the Industrial Power Converter Committee of the IEEE Industry Applications Society.

Zhibin Ling (M'12) received the B.S. and M.S. degrees in electrical engineering from Harbin Science and Technology University, China in 1997 and 2000, respectively, and the Ph.D. degree in electrical engineering from Shanghai Jiao Tong University, China in 2004.

He has been with Shanghai Jiao Tong University since 2004, where he is currently an Associate Professor. He has been PI in externally funded research sponsored by the National Science Foundation of China, Ministry of Science and Technology, and several utilities. He has authored over 50 technical articles, one book chapters, and has obtained 15 patents. His research interests include battery energy storage, renewable power generation, AC/DC hybrid power grid, DC grid, and power electronics applications in power system.

Yihua Hu (M'13-SM'15) received the B.S. degree in electrical motor drives in 2003, and the Ph.D. degree in power electronics and drives in 2011, both from China University of Mining and Technology, Jiangsu, China.

Between 2011 and 2013, he was with the College of Electrical Engineering, Zhejiang University as a Postdoctoral Fellow. Between November 2012 and February 2013, he was an academic visiting scholar with the School of Electrical and Electronic Engineering, Newcastle University, Newcastle upon Tyne, UK. Between 2013 and 2015, he worked as a Research Associate at the power electronics and motor drive group, the University of Strathclyde. Currently, he is a Lecturer at the Department of Electrical Engineering and Electronics, University of Liverpool. He has published more than 35 peer reviewed technical papers in leading journals. His research interests include PV generation system, power electronics converters & control, and electrical motor drives.

Jianhua Wu received the B.S. degree from Nanjing University of Aeronautics and Astronautics, China, and the M.S. and Ph.D. degrees from Huazhong University of Science and Technology, China, in 1983, 1991 and 1994, respectively, all in electrical engineering.

From 1983 to 1989, he was with Guiyang Electric Company as a Design Engineer. Since 2005, He has been a Professor at the College of Electrical Engineering, Zhejiang University, China. He developed the motor design software Visual EMCAD, which is widely used in China. His research interests are electric machine design and drives, including switched reluctance motors, permanent magnet machines for electric vehicle applications.

Dr. Wu is serving as the member of Electrical Steel of Chinese Society for Metals, the Small-power Machine Committee of China Electrotechnical Society, and the Standardization Administration of China.

0278-0046 (c) 2017 IEEE. Personal use is permitted, but republication/redistribution requires IEEE permission. See http://www.ieee.org/publications_standards/publications/rights/index.html for more information.